Progress In Electromagnetics Research, PIER 76, 299–326, 2007

COMPLEX ANALYSIS OF THE INDUCED CURRENTS ON A PERFECTLY CONDUCTING PLANE UNDER COMPLEX BEAM INCIDENCE

M. J. González-Morales

Dpto. Teoría de la Señal y Comunicaciones e I. T.
Universidad de Valladolid
Campus Miguel Delibes, 47011 Valladolid, Spain

E. Gago-Ribas

Dpto. Ingeniería Eléctrica, Electrónica, de Computadores y de Sistemas, Universidad de Oviedo
Campus de Viesques, 33204 Gijón, Spain

C. Dehesa-Martínez

Dpto. Teoría de la Señal y Comunicaciones e I. T.
Universidad de Valladolid
Campus Miguel Delibes, 47011 Valladolid, Spain

Abstract—This paper is concerned with the analysis of the currents induced on a 2D infinite perfectly conducting plane illuminated by a complex beam obtained from the analytical continuation of the real location of a unit impulse source into a complex one. The main goal considering this well-known problem is to understand the meaning of the analytical continuation and the physical information underlying the complex quantities arising from it, and to investigate the capabilities of operating in complex spaces instead of the original real ones through a simple example. Several complex quantities directly related to this problem are analysed and translated into the real domain, leading to a clear and general description of all the possible behaviours of the currents. These results will provide some new insight to extend the complex analysis methodology to more complicated scattering problems. As expected, complex analysis appears to be a full-meaning tool to obtain parameterizations of EM problems, leading to more general solutions and their physical descriptions.

1. INTRODUCTION

In the last three decades, many analytical/numerical techniques have been successfully developed and implemented to investigate a large number of very important problems in electromagnetics, leading to solutions that opened the possibility for analysing more and more complicated structures. As an alternative way, some authors have proposed a kind of *coming back to basics philosophy* that may be able to propose new techniques or revise old ones with a basic aim in mind: to obtain more general solutions which may contain the old ones and even include new solutions, and also that may provide new ways of understanding which enable one to obtain a deeper insight from the physical point of view.

This paper is devoted to present a concrete example of this philosophy, concerning the analytical continuation of the real location of a unit impulse source into a complex one (already proposed in the late 60's and the 70's; refer, for instance, to [1, 2]), and the corresponding analytical continuation of the Green's function of real coordinates into complex coordinates, leading to *complex* radiation and propagation spaces. This procedure has been successfully applied to a wide variety of electromagnetic problems, specially those dealing with Gaussian beams, [3, 4]. (Let us state that there are other approachesto formulate Gaussian Beams [5]). Examples [3] and [4] only use the analytical continuation as a mathematical tool, and do not include an in-depth study of the complex quantities which appear and the physical information underlying on them. Alternative ideas about using complex coordinates and spaces have been set forth in [6] and references therein. From several years ago the authors concentrated their efforts on a thorough investigation of the analytical continuation, [7], and the capabilities of operating in the complex spaces instead of the original real ones. As a result, a parameterization of several complex quantities was obtained, together with a classification of the solutions for the 2D free-space radiation problem [8–10]: the *space of complex distances*, the *space of complex angles*, and the classification of the *complex beams* and their approximations. The complex distance quantity analysed in [8] has been recently used also by other authors; let us mention, for instance, [11] and [12].

Those first studies led us to investigate the possibilities of the complex analysis methodology applied to concrete scattering problems. As a first approach, this paper deals with the induced currents on a very simple and well known structure (a 2D infinite perfectly conducting plane) illuminated by a complex beam, allowing one to concentrate on the meaning and possibilities associated to the complex analysis (which

has unquestionable usefulness in a wide variety of problems [13–15]). New references. In Section 2, the scattering scenario and the incident field are presented. In Section 3, the induced current density on the plane and the classification of its approximations are obtained. The parameterization of the real observation conductor plane in terms of the space of complex distances, as well as other useful complex planes are summarized in Section 4, (details are shown in an appendix). In Section 5, the behaviour of the currents is analysed by *learning to read* the complex parameterizations, which are essential to clearly identify the behaviour of any solution, and the regions where these solutions are valid.

As a conclusion, the results suggest that it is possible to extend this complex analysis methodology to concrete scattering problems (for instance the sort of problems in [16–18]) including more general solutions, their interpretation in terms of complex quantities, complex scattering laws, etc. This also leads to a very important coming back to basics procedure described under the general terminology of *complex signal theory* currently under investigation [19].

2. INCIDENT FIELD

The scenario is described in Fig. 1. A two-dimensional *complex beam*, the axis of which is denoted by ξ, propagating in free space, illuminates a perfect electric conductor (PEC) plane, placed on $z = 0$ and which extends from $-\infty$ to $+\infty$ on the x-direction. A complex beam can be obtained from the field radiated by an infinite line source along y-direction, located at the real position S, with coordinates (x_s, z_s), by the mere translation of the real source by an imaginary displacement, $i\vec{b}$, $\vec{b}$ being a real vector in the same direction as the desired beam axis ξ. A short review of the 2D complex beam concept follows. Time-harmonic dependence $\exp(-i\omega t)$ is assumed throughout this paper.

Start by considering an infinite line source either with an electric current, I_{e}, or a magnetic current, I_{m}. The solutions for the longitudinal field components of the corresponding TE and TM polarized fields (see the sketches in Fig. 1) are given by

$$\begin{aligned} E_y^{\mathrm{ie}} &= \frac{-\omega\mu_0 I_{\mathrm{e}}}{4} H_0^{(1)}(k_0 R_{\mathrm{s}}), \\ H_y^{\mathrm{im}} &= \frac{-\omega\varepsilon_0 I_{\mathrm{m}}}{4} H_0^{(1)}(k_0 R_{\mathrm{s}}), \end{aligned} \tag{1}$$

where $R_{\mathrm{s}} = \sqrt{(x - x_s)^2 + (z - z_s)^2}$ is the the real distance from an observation point (x, z) to the source location (x_s, z_s).

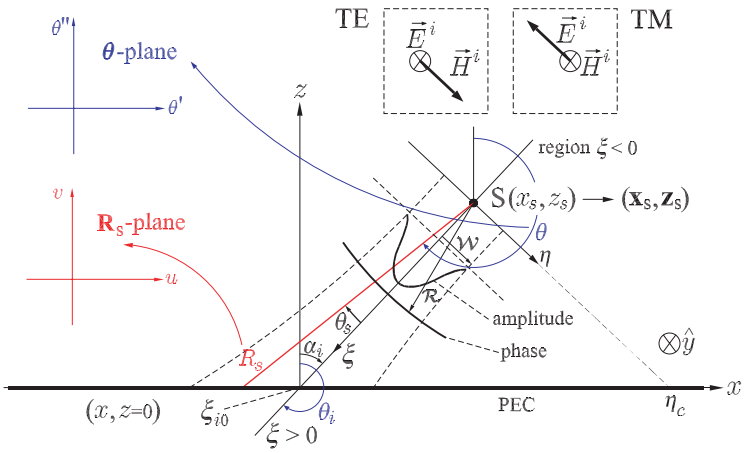

Figure 1. Geometry of a beam incidence on a plane. When the source real position is analytically extended to a complex one, the cylindrical field wave becomes a complex beam, which can be referred to a natural coordinate system (ξ, η). Real distances and angles become complex.

When the line source is moved from its real position (x_s, z_s) to the complex one $(\mathbf{x_s}, \mathbf{z_s})$, given by[†]

$$\begin{aligned} \mathbf{x_s} &= x_s + ib\sin\theta_i = x_s - ib\sin\alpha_i, \\ \mathbf{z_s} &= z_s + ib\cos\theta_i = z_s - ib\cos\alpha_i, \end{aligned} \tag{2}$$

the field components obtained from that of the real-located source by replacing the real distance, R_s, by the *Complex Distance*, $\mathbf{R_s}$, defined by [8, 9]

$$\mathbf{R_s} = \sqrt{(x - \mathbf{x_s})^2 + (z - \mathbf{z_s})^2}, \tag{3}$$

are also solutions of the wave equation. (Since Eq. (3) defines a multivalued function, the condition $\Re\{\mathbf{R_s}\} \geq 0$ must be imposed so that the radiated far field is an outgoing wave.) Such field configurations are called *Complex Beams*, (CB) [1, 2]. In Eq.˙ (2), the angles α_i or $\theta_i = \pi + \alpha_i$ define the beam axis direction, and b is related to the usual Gaussian beam waist width, $\mathcal{W}$ (see Fig. 1). In particular, the TE polarized wave fields radiated by a line of electric

[†] Notice that vectors are distinguished by an arrow, as $\vec{b}$. Symbols in boldface, as $\mathbf{x_s}$ or $\mathbf{R_s}$, represent those complex quantities which appear in the formulation of complex beams directly related to corresponding real quantities arising in the formulation of the original cylindrical wave, as x_s or R_s.

current $I_{\rm e}$ placed at the complex position $(\mathbf{x_s}, \mathbf{z_s})$ are given by the following expressions,

$$\begin{aligned} E_y^{\rm ie} &= \frac{-I_{\rm e}\omega\mu_0}{4} H_0^{(1)}(k_0\mathbf{R_s}), \\ H_x^{\rm ie} &= \frac{-1}{i\omega\mu_0}\frac{\partial E_y^{\rm i}}{\partial z} = \frac{I_e i k_0}{4}\mathbf{R}'_{\mathbf{s}z} H_1^{(1)}(k_0\mathbf{R_s}), \\ H_z^{\rm ie} &= \frac{1}{i\omega\mu_0}\frac{\partial E_y^{\rm i}}{\partial x} = \frac{-I_{\rm e} i k_0}{4}\mathbf{R}'_{\mathbf{s}x} H_1^{(1)}(k_0\mathbf{R_s}), \end{aligned} \tag{4}$$

where the derivatives

$$\begin{aligned} \mathbf{R}'_{\mathbf{s}z} &= \frac{\partial \mathbf{R_s}}{\partial z} = \frac{z - \mathbf{z_s}}{\mathbf{R_s}} = \cos\boldsymbol{\theta}, \\ \mathbf{R}'_{\mathbf{s}x} &= \frac{\partial \mathbf{R_s}}{\partial x} = \frac{x - \mathbf{x_s}}{\mathbf{R_s}} = \sin\boldsymbol{\theta}, \end{aligned} \tag{5}$$

introduce the *Complex Angle*, $\boldsymbol{\theta}$. Their detailed parameterization may be found in [9].

By following a similar procedure, the TM polarized CB incident field radiated by an infinite line of magnetic current $I_{\rm m}$ localized at $(\mathbf{x_s}, \mathbf{z_s})$ will be given by

$$\begin{aligned} H_y^{\rm im} &= \frac{-I_{\rm m}\omega\varepsilon_0}{4} H_0^{(1)}(k_0\mathbf{R_s}), \\ E_x^{\rm im} &= \frac{1}{i\omega\varepsilon_0}\frac{\partial H_y^i}{\partial z} = \frac{-I_{\rm m} i k_0}{4}\mathbf{R}'_{\mathbf{s}z} H_1^{(1)}(k_0\mathbf{R_s}), \\ E_z^{\rm im} &= \frac{-1}{i\omega\varepsilon_0}\frac{\partial H_y^i}{\partial x} = \frac{I_{\rm m} i k_0}{4}\mathbf{R}'_{\mathbf{s}x} H_1^{(1)}(k_0\mathbf{R_s}). \end{aligned} \tag{6}$$

3. INDUCED CURRENT DENSITY

The usual physical optics approximation for the induced surface current density becomes an *exact solution* when applied to an infinite perfect electric conductor plane, and it is given by the expression $\vec{J} = 2\hat{z} \times \vec{H}^{\rm i}$ $(z = 0)$. The corresponding expressions for the considered TE and TM polarizations become now,

$$\begin{aligned} \vec{J}^{\rm e} &= J_y^{\rm e}\ \hat{y} = 2H_x^{\rm ie}\ \hat{y}, \quad z = 0, \\ \vec{J}^{\rm m} &= J_x^{\rm m}\ \hat{x} = -2H_y^{\rm im}\ \hat{x}, \quad z = 0. \end{aligned} \tag{7}$$

Real-source solution

By using (1) and (7), it is possible to write the *exact solutions*,

$$\begin{aligned} J^{\mathrm{e}}_{y,\mathrm{RS}} &= \frac{I_{\mathrm{e}} i k_0}{2} R'_{\mathrm{s}0} H^{(1)}_1(k_0 R_{\mathrm{s}0}), \\ J^{\mathrm{m}}_{x,\mathrm{RS}} &= \frac{\omega \varepsilon_0 I_{\mathrm{m}}}{2} H^{(1)}_0(k_0 R_{\mathrm{s}0}), \end{aligned} \tag{8}$$

where $R_{\mathrm{s}0}$ and $R'_{\mathrm{s}z0}$ identify the quantities R_{s} and $R'_{\mathrm{s}z} = \partial R_{\mathrm{s}z}/\partial z$, respectively, both particularized on the $z = 0$ plane.

Under High Frequency–Far Field (*HF-FF*) condition, $k_0 R_{\mathrm{s}} \gg 1$, and using the asymptotic expression for the Hankel function [20], the previous equations reduce to

$$\begin{aligned} J^{\mathrm{e}}_{y,\mathrm{FF,RS}} &\sim \frac{I_{\mathrm{e}} k_0 z_s e^{i3\pi/4}}{\sqrt{2\pi}} \frac{e^{ik_0 R_{\mathrm{s}0}}}{R_{\mathrm{s}0}\sqrt{k_0 R_{\mathrm{s}0}}}, \\ J^{\mathrm{m}}_{x,\mathrm{FF,RS}} &\sim \frac{I_{\mathrm{m}} \omega \varepsilon_0 e^{-i\pi/4}}{\sqrt{2\pi}} \frac{e^{ik_0 R_{\mathrm{s}0}}}{\sqrt{k_0 R_{\mathrm{s}0}}}. \end{aligned} \tag{9}$$

Complex-source solution

Based on the classification of the different field solutions generated by a complex source, [9, 10], it is also possible to classify the induced currents as it follows.

From (7), together with Eqs. (4)–(6), it is possible to write the *exact solutions* in the form,

$$\begin{aligned} J^{\mathrm{e}}_{y,\mathrm{CB}} &= \frac{I_{\mathrm{e}} i k_0}{2} \mathbf{R'_{sz0}} H^{(1)}_1\left(k_0 \mathbf{R_{s0}}\right), \\ J^{\mathrm{m}}_{x,\mathrm{CB}} &= \frac{I_{\mathrm{m}} \omega \varepsilon_0}{2} H^{(1)}_0\left(k_0 \mathbf{R_{s0}}\right). \end{aligned} \tag{10}$$

Notice that the expressions in (10) include the complex distance $\mathbf{R_{s0}} = \mathbf{R_s}(x, z = 0)$, as well as the complex quantity $\mathbf{R'_{sz0}} = \cos\boldsymbol{\theta}(x, z = 0)$ which appears due to the complex continuation in (2).

For a complex beam, the *complex HF-FF condition*, $k_0 |\mathbf{R_s}| \gg 1$, can be used to define a boundary of validity of such a condition,

$$k_0 |\mathbf{R_s}| = M_{\mathrm{CFF}}, \tag{11}$$

where $M_{\mathrm{CFF}} \gg 1$ is a conventionally chosen criterion. For points in that region, the asymptotic approximation to the complex beam is referred to as Far Field Complex Beam (FFCB), [10], and the surface

currents in (10) reduce to

$$J^{\mathrm{e}}_{y,\mathrm{FFCB}} \sim \frac{I_{\mathrm{e}} k_0 \mathbf{z_s} e^{i3\pi/4}}{\sqrt{2\pi k_0}} \frac{e^{ik_0 \mathbf{R_{s0}}}}{\mathbf{R}_{\mathbf{s0}}^{3/2}},$$
$$J^{\mathrm{m}}_{x,\mathrm{FFCB}} \sim \frac{I_{\mathrm{m}} \omega \varepsilon_0 e^{-i\pi/4}}{\sqrt{2\pi}} \frac{e^{ik_0 \mathbf{R_{s0}}}}{\sqrt{k_0 \mathbf{R_{s0}}}}. \tag{12}$$

Notice that equations (10) and (12) reduce to those in (8) and (9) when $b = 0$, as expected.

The paraxial beam region can be defined in the beam-adapted coordinate system (ξ, η), as sketched in Fig. 1, by the expression

$$\frac{\xi^2 + b^2}{\eta^2} = M_{\mathrm{par}}, \tag{13}$$

where $M_{\mathrm{par}} \gg 1$ is a conventionally chosen criterion. In that region, the FFCB solution turns into a Gaussian Beam (GB) incident field, [2], and the paraxial approximations of the surface currents densities are given by

$$J^{\mathrm{e}}_{y,\mathrm{GB}} \sim \frac{I_{\mathrm{e}} k_0 \mathbf{z_s} e^{i3\pi/4} e^{k_0 b}}{\sqrt{2\pi k_0}} \frac{e^{\frac{-\eta_0^2}{\mathcal{W}^2(\xi_0)}} e^{ik_0\left(\xi_0 + \frac{\eta_0^2}{2\mathcal{R}(\xi_0)}\right)}}{(\xi_0 - ib)^{3/2}},$$
$$J^{\mathrm{m}}_{x,\mathrm{GB}} \sim \frac{I_{\mathrm{m}} \omega \varepsilon_0 e^{-i\pi/4} e^{k_0 b}}{\sqrt{2\pi}} \frac{e^{\frac{-\eta_0^2}{\mathcal{W}^2(\xi_0)}} e^{ik_0\left(\xi_0 + \frac{\eta_0^2}{2\mathcal{R}(\xi_0)}\right)}}{\sqrt{k_0(\xi_0 - ib)}}, \tag{14}$$

where $\mathcal{W}^2(\xi_0)$ and $\mathcal{R}(\xi_0)$ are, respectively, the width squared and the curvature radius of the Gaussian beam, i.e.,

$$\mathcal{W}^2(\xi_0) = \frac{2b}{k_0}\left(1 + \frac{\xi_0^2}{b^2}\right), \quad \mathcal{R}(\xi_0) = \frac{\xi_0^2 + b^2}{\xi_0}. \tag{15}$$

Notice that (ξ_0, η_0) in (14)–(15) are the values of the beam-adapted coordinates on the plane $z = 0$, that is $\xi_0(x) = \xi(x, z = 0)$ and $\eta_0(x) = \eta(x, z = 0)$.

For some analytical and practical applications it may be useful to consider only the phase function dominant terms of the FFCB and the GB solutions, leading to new approximated *HF-FF* solutions. For the FFCB, denoting $\mathbf{R_{s0}} = u_0 + iv_0$, and suppressing constant terms, the total phase in (12) is given by $k_0 u_0 + \varphi^{\mathrm{e}}$, and $k_0 u_0 + \varphi^{\mathrm{m}}$, respectively,

with $\varphi^{\mathrm{e}} = -\frac{3}{2}\tan^{-1}(v_0/u_0)$, and $\varphi^{\mathrm{m}} = -\frac{1}{2}\tan^{-1}(v_0/u_0)$. Under *HF-FF* condition,

$$M_{\mathrm{EP}} = \frac{k_0 u_0}{\varphi^{\mathrm{e,m}}} \gg 1, \tag{16}$$

and the shape of the lines of constant phase in the FFCB solution becomes elliptic; this solution is denoted as EP-FFCB,

$$\begin{aligned} J^{\mathrm{e}}_{y,\text{EP-FFCB}} &\sim I_{\mathrm{e}} k_0 \mathbf{z_s} \frac{e^{i3\pi/4}}{\sqrt{2\pi k_0}} \frac{e^{ik_0 \mathbf{R_{s0}}}}{|\mathbf{R_{s0}}|^{3/2}}, \\ J^{\mathrm{m}}_{x,\text{EP-FFCB}} &\sim I_{\mathrm{m}} \omega \varepsilon_0 \frac{e^{-i\pi/4}}{\sqrt{2\pi k_0}} \frac{e^{ik_0 \mathbf{R_{s0}}}}{|\mathbf{R_{s0}}|^{1/2}}. \end{aligned} \tag{17}$$

Finally, for the GB solution, the total phase in (14), again neglecting constant terms, is given by $\varphi_l + \varphi_c + \varphi^{\mathrm{e}}$ and $\varphi_l + \varphi_c + \varphi^{\mathrm{m}}$, respectively, with $\varphi_l = k_0\xi_0$, $\varphi_c = k_0\eta_0^2/2\mathcal{R}(\xi_0)$, $\varphi^{\mathrm{e}} = -\frac{3}{2}\tan^{-1}(b/\xi_0)$, and $\varphi^{\mathrm{m}} = -\frac{1}{2}\tan^{-1}(b/\xi_0)$. Under *HF-FF* condition,

$$M_{\mathrm{SP}} = \frac{\varphi_l}{\varphi_c + \varphi^{\mathrm{e,m}}} \gg 1, \tag{18}$$

and the shape of the lines of constant phase of the GB solution becomes straight; this solution is denoted as SP-GB,

$$\begin{aligned} J^{\mathrm{e}}_{y,\text{SP-GB}} &\sim I_{\mathrm{e}} k_0 \mathbf{z_s} \frac{e^{i3\pi/4} e^{k_0 b}}{\sqrt{2\pi k_0}} \frac{e^{\frac{-\eta_0^2}{\mathcal{W}^2(\xi_0)}} e^{ik_0\xi_0}}{(\xi_0^2 + b^2)^{3/4}}, \\ J^{\mathrm{m}}_{x,\text{SP-GB}} &\sim I_{\mathrm{m}} \omega \varepsilon_0 \frac{e^{-i\pi/4} e^{k_0 b}}{\sqrt{2\pi k_0}} \frac{e^{\frac{-\eta_0^2}{\mathcal{W}^2(\xi_0)}} e^{ik_0\xi_0}}{(\xi_0^2 + b^2)^{1/4}}. \end{aligned} \tag{19}$$

The whole classification of the solutions for the current in the conductor is outlined in Fig. 2. Only the GB solutions in (14) and (19) are commonly used in most scattering problems, missing the possibilities associated to the general *complexification* procedure.

4. REAL AND COMPLEX SPACES

Since the fields in Eqs. (4) and (6) and the induced currents in Eqs. (10) and (12) depends in a natural way on the complex distance, $\mathbf{R_s}$, and eventually on its z-derivative, i.e., $\cos\boldsymbol{\theta}$, it is interesting to carry out their analysis in terms of these complex variables. For that purpose,

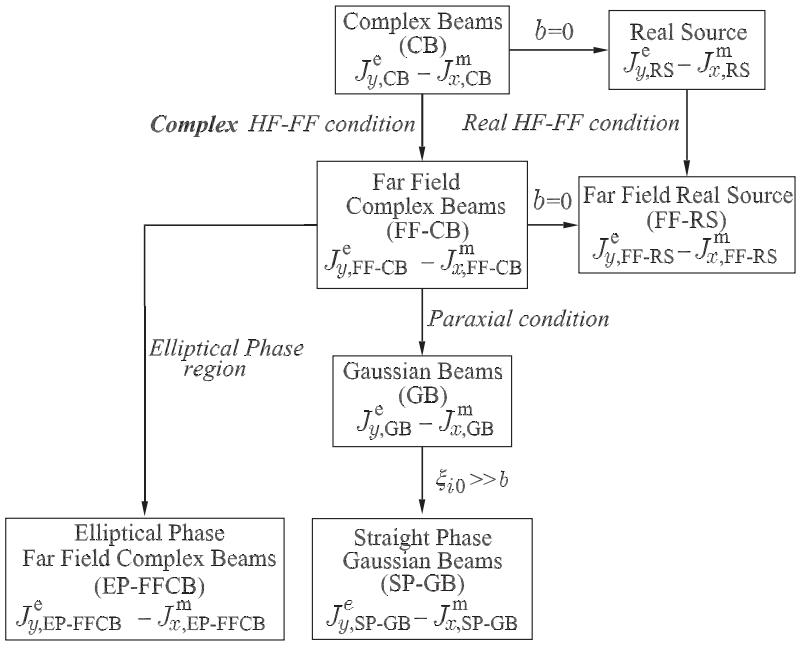

Figure 2. Classification of the field solutions and the corresponding currents. The exact solution is related to the CB incident field. Under *complex HF-FF condition*, the currents will be associated with the FFCB field solution. Applying also the *paraxial condition*, the currents will be related to a GB. The formulation reduces to the well known real case by making $b = 0$. In this case, the exact solution and the solution under *HF-FF condition* will be related to the Hankel function of real argument and its asymptotic solution, respectively.

we introduce the Space of Complex Distances (SCD), defined as the complex plane $\mathbf{R_s} = u + iv$, where $\mathbf{R_s}$ was defined in Eq.(3), but parameterized in terms of the beam-adapted real coordinates (ξ, η), see Fig. 1, as

$$\mathbf{R_s} = \sqrt{\xi^2 + \eta^2 - b^2 - 2ib\xi}. \tag{20}$$

As remarked after the definition in Eq.(3), $\Re\{\mathbf{R_s}\} = u \geq 0$ must be chosen; $\Im\{\mathbf{R_s}\} = v \lessgtr 0$ corresponds to $\xi \gtrless 0$, half planes.

The presence of the square root in $\mathbf{R_s}$ suggests the introduction of an auxiliary Space of Complex Distance Squared (SCDS), $\mathbf{q} =$

$q' + iq'' = \mathbf{R}_\mathbf{s}^2$. The mapping between the SCD and the SCDS is given by

$$\mathbf{R}_\mathbf{s} = u + iv \rightarrow \begin{cases} u = \dfrac{1}{\sqrt{2}}\sqrt{|\mathbf{q}| + q'}, \\ v = \mp\dfrac{1}{\sqrt{2}}\sqrt{|\mathbf{q}| - q'}. \end{cases} \tag{21}$$

On the other hand, the mapping between the SCDS and the real space, represented in terms of the coordinates (ξ, η), is

$$\mathbf{q} = \mathbf{R}_\mathbf{s}^2 = q' + iq'' \rightarrow \begin{cases} q' = \xi^2 + \eta^2 - b^2, \\ q'' = -2b\xi. \end{cases} \tag{22}$$

Finally, the analysis of the $\cos\boldsymbol{\theta}$-plane defined in (5) is made by denoting

$$\cos\boldsymbol{\theta} = \gamma' + i\gamma'', \tag{23}$$

and substituting $z - \mathbf{z}_\mathbf{s} = z - z_s + ib\cos\alpha_i$, and $\mathbf{R}_\mathbf{s}^{-1} = u/(u^2 + v^2) - iv/(u^2 + v^2)$, leading to the parametric equations,

$$\begin{cases} \gamma' = (z - z_s)\dfrac{u}{u^2 + v^2} + b\cos\alpha_i\dfrac{v}{u^2 + v^2}, \\ \gamma'' = (z - z_s)\dfrac{-v}{u^2 + v^2} + b\cos\alpha_i\dfrac{u}{u^2 + v^2}, \\ z - z_s = -\xi\cos\alpha_i - \eta\sin\alpha_i. \end{cases} \tag{24}$$

A detailed analysis of these parameterizations may be found in [9]. Some of those results are applied here and new parameterizations directly related to the problem under analysis are introduced. Specifically, (i) the characterization of the $z = 0$ plane which constitutes the set of real observation points where the currents are defined, and (ii) the characterization of the back region of the beam ($\xi < 0$) which will appear from the intersection between the plane and the η-axis.

The parameterization of the real observation points in the SCD will be essential to analyse the behaviour of the induced currents on the plane. Four examples showing some configurations of the incident beam for a fixed value of the real distance from the origin to the real source position, ξ_{i0}, and for different values of the incidence angle, α_i, appear in Fig. 3. The plots show, for each case, curves defining regions of validity of the *complex HF-FF* and *paraxial* conditions [refer to Eqs. (11) and (13), respectively], i.e., the loci of constant M_{CFF} and

$M_{\rm par}$. Fig. 4 collects all these results on (a) the SCDS and (b) the SCD, together with the curves representing the real observation points on the plane, for different values of α_i. For the missing details, the reader is referred to Appendix A, where a sketch of the analysis of the $\cos\boldsymbol{\theta}$-plane, which constitutes a term of the currents in (10), is also included.

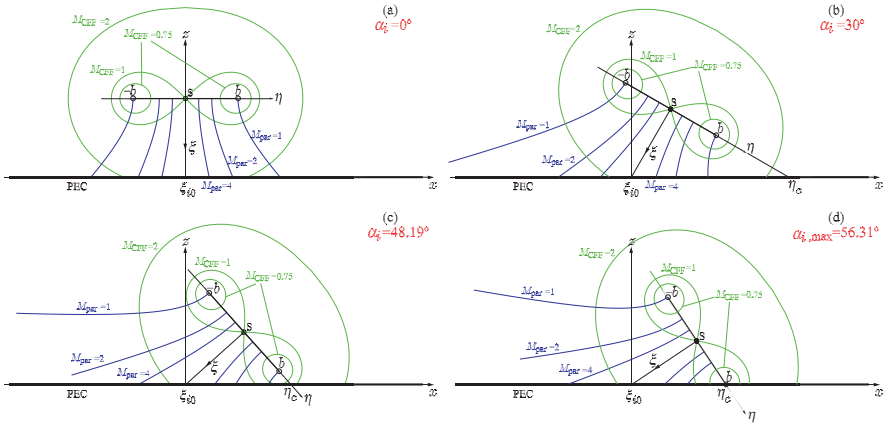

Figure 3. Parameterization of the real propagation space in terms of the *complex HF-FF condition* for $M_{\rm CFF} = 0.75$, 1 and 2, the *paraxial condition*, for $M_{\rm par} = 1$, 2 and 4, and the real observation points, for the normalized value $\xi_{i0n} = \xi_{i0}/b = 1.5$ and $\alpha_i = 0°$ (normal incidence), 30°, 48.19° and $\alpha_{i,\max} = 56.31°$.

5. ANALYSIS OF THE CURRENTS

5.1. Exact solution and ranges of the approximations

Even though we will later concentrate on the asymptotic approximation related to the FFCB incidence, first, we will briefly refer to the exact solution in (10) related to *complex beam* incidence, which is necessarily needed to validate any approximation in Fig. 2. The exact solution is determined by the functions $H_1^{(1)}(k_0\mathbf{R_{s0}})$ and $\cos\boldsymbol{\theta}$ for TE polarization, and by the function $H_0^{(1)}(k_0\mathbf{R_{s0}})$ for TM polarization. In Fig. 5, the dependence of $\left|J^{\rm m}_{x,\rm CB}\right|$, (TM case) on the (u, v) coordinates of the SCD is depicted for the four values of the incidence angle α_i chosen in Fig. 3. In this way, the behaviour of the TM currents may be understood and interpreted on the SCD.

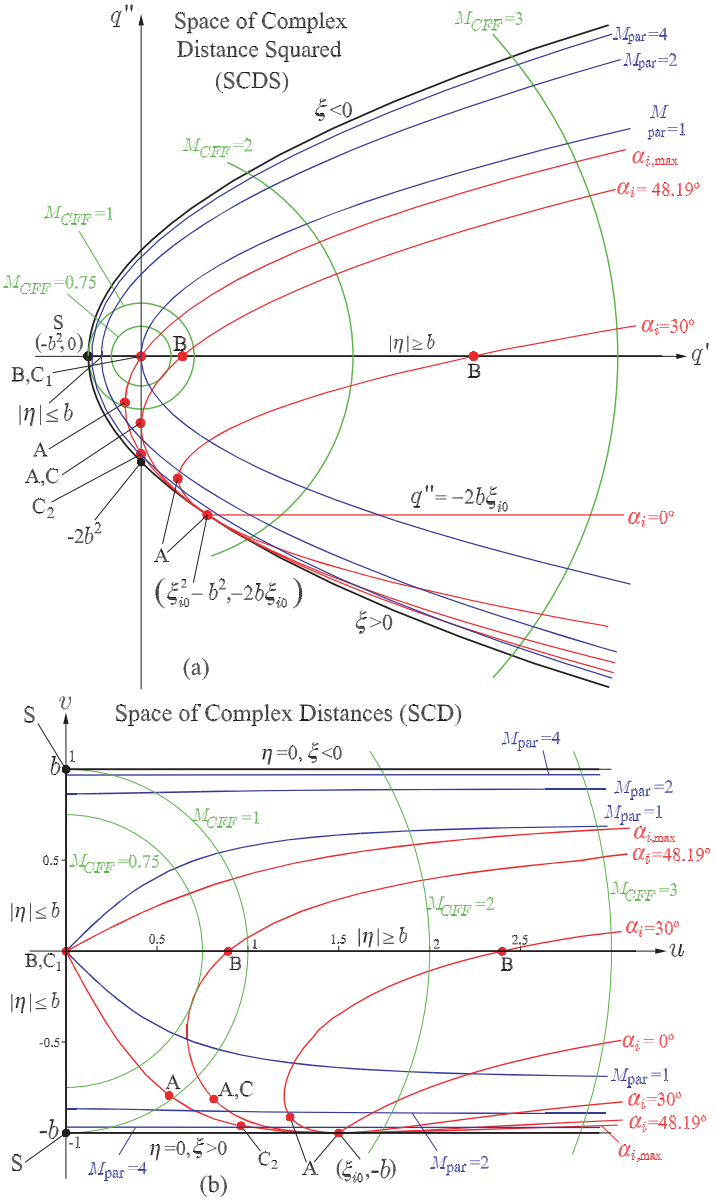

Figure 4. Parameterization of (a) the Space of Complex Distances Squared, and (b) the Space of Complex Distances, in terms of curves with constant values of M_{CFF} and M_{par}, and the points of the conducting plane, for the values of α_i shown in Fig. 3.

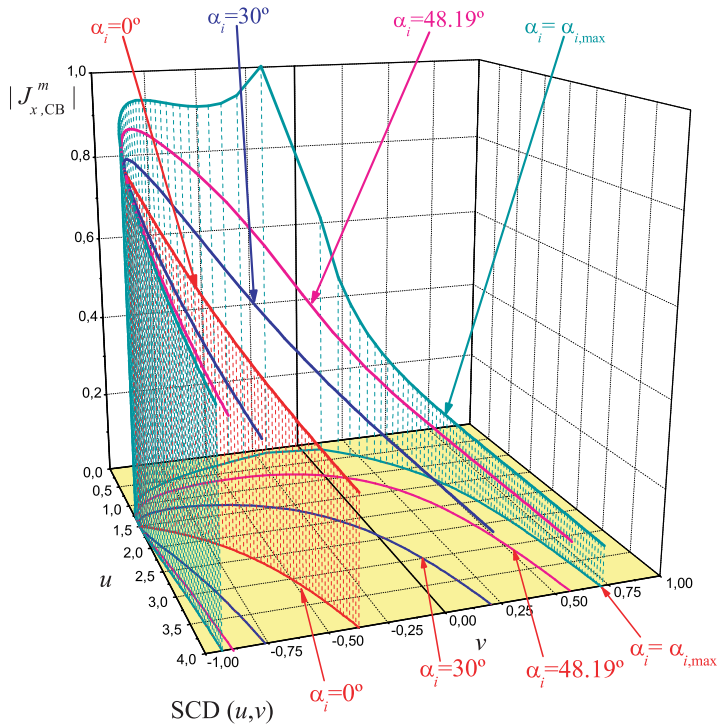

Figure 5. Amplitude of the exact current for TM polarization in the SCD for the particular examples presented in Figs. 3 and 4. This example is only $\mathbf{R_{s0}}$–dependent.

Concerning to $J_y^e(x)$ in (10) (TE case), Figs. 6, 7 and 8 show three examples of the analysis in the SCD, the values on the $\cos\boldsymbol{\theta}$-plane and the corresponding behaviour of the currents on the real observation points. (Values of $H_1^{(1)}(k_0\mathbf{R_{s0}})$ on the (u, v) plane have been omitted for simplicity). The CB reference solution in (10) is compared with the solutions under *complex HF-FF* and *paraxial* approximations. The values of the relative errors correspond to $M_{\text{CFF}} = 2$ and $M_{\text{par}} = 4$, considering the examples with $\alpha_i = 48.19°$ in Fig. 6, $\alpha_i = 0°$ in Fig. 7, and $\alpha_i = \alpha_{i,\max} = 56.31°$ in Fig. 8. The relative position of the real source S with respect to dimension b is given by $\xi_{i0n} = \xi_{i0}/b = 1.5$, and the current value $I_e = 1$ A.

The example in Fig. 6 ($\alpha_i = 48.19°$) shows that the FFCB currents will be a valid solution in the region from $x \to -\infty$ to point A. Only the currents under CB incidence will be a valid solution in the region from points A to B (region within $M_{\text{CFF}} = 2$ and outside $M_{\text{par}} = 4$).

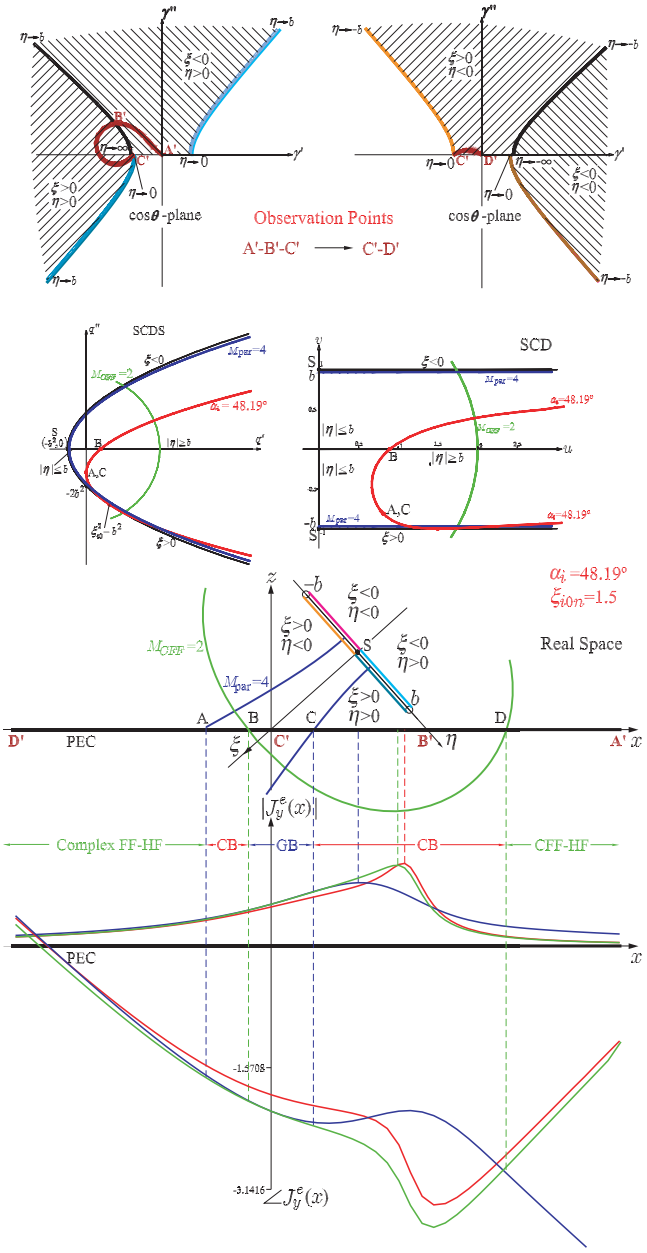

Figure 6. Amplitude and phase analysis of the TE-current induced on the plane for $\alpha_i = 48.19°$, $\xi_{i0n} = \xi_{i0}/b = 1.5$ and $I_e = 1$ A. The validity regions associated with different approximations (CB, FFCB and GB) are indicated by points A-B-C-D. See the text for details.

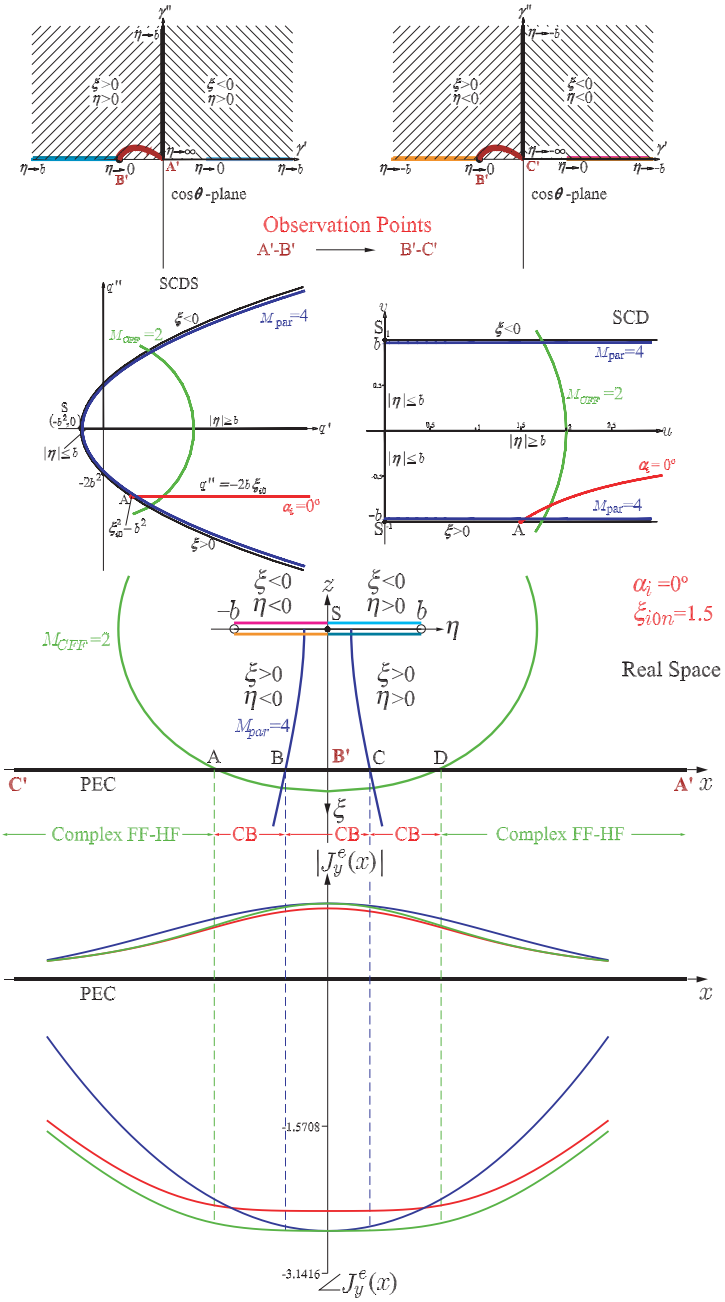

Figure 7. Amplitude and phase analysis of the TE-currents induced on the plane for normal incidence, $\alpha_i = 0°$ and $\xi_{i0n} = \xi_{i0}/b = 1.5$.

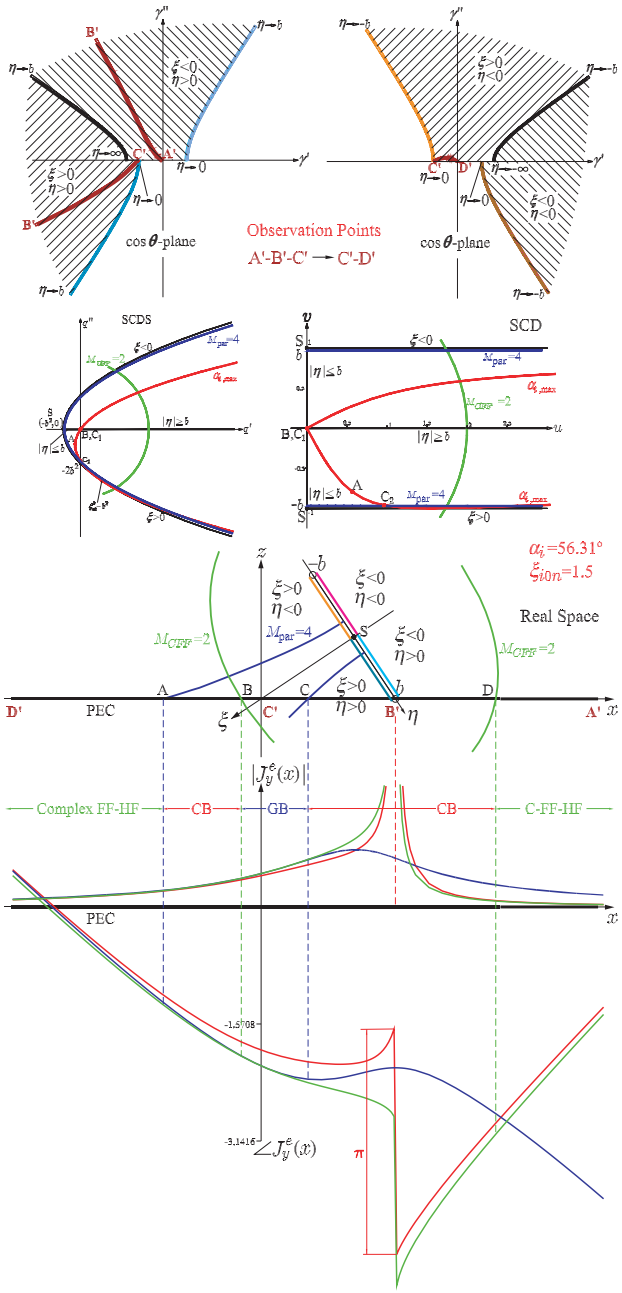

Figure 8. Amplitude and phase analysis of the TE-currents induced on the plane for $\alpha_i = \alpha_{i0,\max} = 56.31°$ and $\xi_{i0n} = \xi_{i0}/b = 1.5$.

From point B to C, the GB currents will be a valid solution since all the portion is located within the regions delimited by $M_{\mathrm{CFF}} = 2$ and $M_{\mathrm{par}} = 4$ simultaneously. The situation in the region from point C to D is similar to that from A to B, and only the CB currents solution will be valid. Finally, the situation from D to $x \to +\infty$ makes the FFCB solution to be a valid approximation.

Results in Figs. 7 and 8 can be read in a similar manner. Due to the symmetry in Fig. 7, the behaviour of the currents is the same in the semi-plane $x > 0$ and $x < 0$. A special situation occurs in Fig. 8 when the real equivalent distribution of sources touches the plane (point $\eta = b$), where the sign of $\cos\boldsymbol{\theta}$ changes, leading to a currents phase discontinuity of value π.

In relation to the Gaussian beam solution, the paraxial region concentrates close to the line $v = -b$ (positive ξ axis) in the SCD. GB's may be studied as a particular case of the complex analysis, but may be also analysed in terms of the conventional real coordinates as usually used.

5.2. Analysis of the FFCB solution

Let us now concentrate on the asymptotic approximation related to the FFCB incidence for both, TE and TM polarizations. There are two terms in (12) which determine the final behaviour of the induced currents: (i) the exponential term $e^{ik_0\mathbf{R_s}}$, and (ii) terms $\mathbf{R_s}^{-3/2}$ for the TE polarization and $\mathbf{R_s}^{-1/2}$ for the TM polarization. In complex coordinates, both terms (named as *exponential* and *square root terms* in this paper) will contribute to the phase and the amplitude of the final solution. The other terms in (12) remain constant once the source of the incident field has been fixed. Notice that $\cos\boldsymbol{\theta}$ term in (5) is broken down in $\mathbf{R_s}^{-1}$ which is included in the *square root term*, and $\mathbf{z_s}$, which only depends on the source.

Exponential term. $e^{ik_0\mathbf{R_s}}$ may be separated into the amplitude, $e^{-k_0 v}$, and phase, $e^{ik_0 u}$, contributions. From the analysis in the SCD and the information in Fig. 9(a), it is possible to perform the following considerations: (i) The amplitude profile takes its maximum value, $A_{\mathrm{max,exp}}$, at a certain point in the conducting plane identified in the SCD by the point where $v = \Im\{\mathbf{R_s}\}$ reaches its minimum value, $v = -b$, corresponding to the intersection between the plane and the positive ξ-axis parameterizations; this point is unique and independent from α_i. (ii) The phase profile presents a minimum value, $P_{\mathrm{min,exp},\alpha_i}$, at certain α_i-dependent point in the plane identified in the SCD by the point where $u = \Re\{\mathbf{R_s}\}$ reaches its minimum

value. (iii) For points far away from ξ_{i0} ($x \to \infty$), the constant phase curves in the SCD become approximately straight lines, and the phase fronts become circumferences in the real space, which leads to the approximation $\exp(ik_0u) \sim \exp(ik_0\sqrt{\xi^2+\eta^2})$. Under the same conditions, v approaches a constant asymptotic value, $v = \mp b \sin\alpha_i$.

Square root term. The following description will be valid for both TE polarization, where the amplitude and phase contributions from ${\mathbf{R_s}}^{-3/2}$ are given by $(u^2+v^2)^{-3/4}$ and $-\frac{1}{2}\tan^{-1}\frac{v}{u}$, as well as for TM polarization, where the amplitude and phase contributions from ${\mathbf{R_s}}^{-1/2}$ are given by $(u^2+v^2)^{1/4}$ and $-\frac{1}{2}\tan^{-1}\frac{v}{u}$, respectively. The following behaviour may be observed from the plane parameterization in the SCD, Fig. 9(b): (i) The amplitude profile takes its maximum value, $A_{\max,\mathrm{sqr},\alpha_i}$, at points identified in the SCD where u^2+v^2 reaches its minimum value. These points will be localized by considering the tangent points between the family of circumferences $u^2+v^2 =$ constant and the real plane. Its analysis appears more clear in the SCDS where these points may be identified by a explicit equation obtained from the intersection between the parabolas in (A10), identifying the observation plane, and the circumferences $q'^2 + q''^2 =$ constant, leading to a unique point that may be identified graphically[‡]. (ii) The phase profile presents two extreme contributions, the first one corresponding to a positive phase value which leads to the minimum phase contribution, $P_{\min,\mathrm{sqr},\alpha_i}$, and the second one corresponding to a negative phase value which leads to the maximum phase contribution, $P_{\max,\mathrm{sqr},\alpha_i}$. These points may be geometrically characterized by the tangents between the family of straight lines $v = mu$ and the real plane, with $m = \tan\alpha$, $\alpha \gtrless 0$ for $P_{\min,\mathrm{sqr},\alpha_i}$ and $P_{\max,\mathrm{sqr},\alpha_i}$, respectively. Again, the analysis of this problem becomes easier in the SCDS, where the analysis may be performed graphically[§].

Profiles and numerical examples. The last two terms together determine the final behaviour of the current described in (12) and depicted in Figs. 6, 7 and 8. The amplitude has a pseudo-gaussian profile that vanishes far away from the beam axis, and, the phase has a linear profile around the beam axis and grows up as going away from the locations closed to the source. The exponential term will be specially relevant far away from the real position of the source. In fact, this term may become the only significant term for certain analysis,

[‡] The mathematical resolution leads to a fourth degree polynomial equation that may be analytically solved but it is rather advisable to numerically solve.

[§] The mathematical resolution leads to a biquadratic polynomial equation which may be analytically solved for m as $m = [-b_2 \pm (b_2^2 - 4b_1b_3)^{1/2}]/2b_1$, with $b_1 = \xi_{i0}^2/b^2\tan^4\alpha_i$, $b_2 = 2\xi_{i0}/b\tan^2\alpha_i$,and $b_3 = 1 - \xi_{i0}^2\cos^2\alpha_i/b^2\sin^4\alpha_i + 1/\sin^2\alpha_i$.

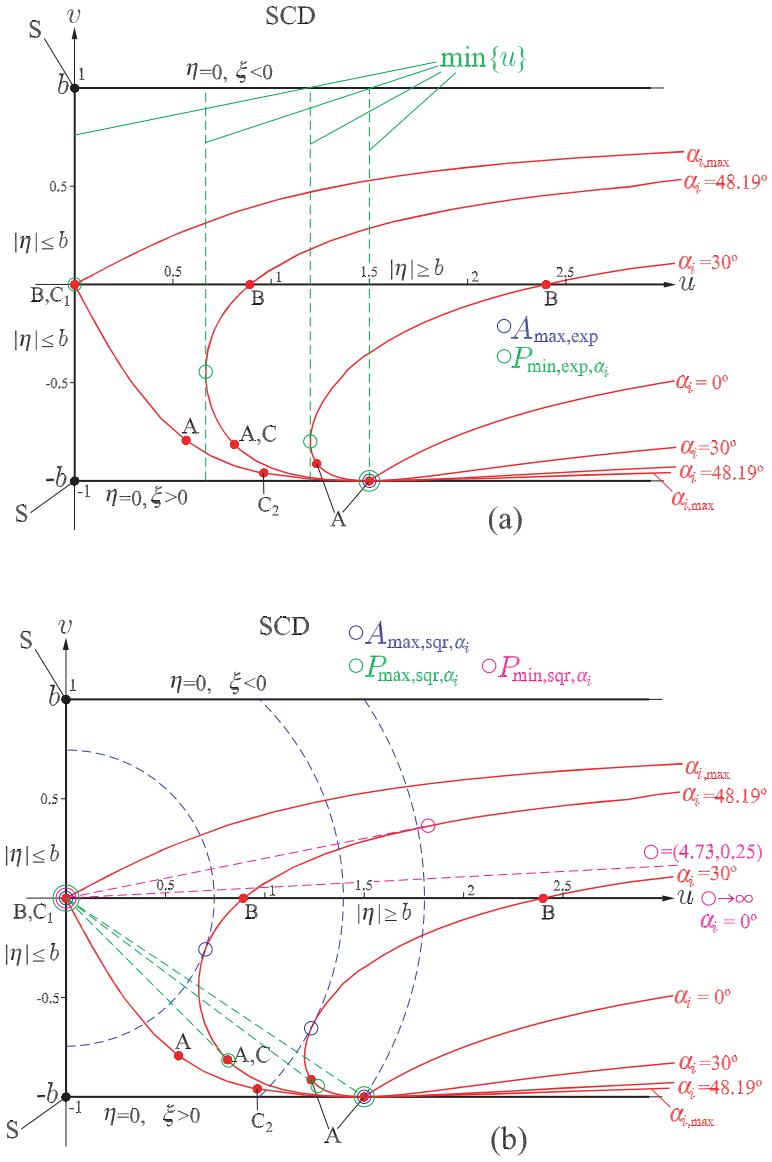

Figure 9. Graphical analysis in the SCD of the amplitude and phase contributions in the FFCB solution from (a) the exponential term, $A_{\max,\exp}$ and $P_{\min,\exp,\alpha_i}$, and (b) the square root term, $A_{\max,\mathrm{sqr},\alpha_i}$, $P_{\max,\mathrm{sqr},\alpha_i}$ and $P_{\min,\mathrm{sqr},\alpha_i}$.

as those concerning the asymptotic evaluation of the radiated field by a current distribution. On the other hand, the square root term is the most significant contribution determining the behaviour of the currents in the near region. Up to our knowledge, it is not possible to find an analytical expression for the maximum amplitude and the minimum phase positions for the final expression with both terms, neither in the real space nor in the SCD. The previous analysis is intended to emphasize the importance of the SCD parameterizations where all the properties associated with any term appear in a clear way enabling one to predict and understand its global behaviour as well as the parameters which determine that behaviour.

6. CONCLUSIONS

The currents induced on a 2D infinite perfect conductor plane when illuminated by a CB generated by a complex-localized source have been studied in detail. From the exact general solution related to the CB incident field, a complete classification of all the possible approximated solutions together with the parameterization of their corresponding validity ranges, have been presented.

The asymptotic approximation under the *complex HF-FF condition*, that is the FFCB solution, has a special relevance as long as it may be validated close to the source physical position, and also because it includes a broad range of field behaviours characterized in terms of the source parameters (k_0, b and α_i). This approximation has been specially emphasized as an example of the operative capabilities associated with several spaces of complex coordinates (SCD, SCDS, ...), as well as to describe the procedure to translate those analyses into the original real space in which the problem is defined. The well known GB solution appears as a particular case of the complex analysis. Through these examples, it is also possible to show the capabilities to solve a much more general problem analytically, and also to gain a deeper understanding of the roles played by the complex quantities associated with the description of a real problem, in particular those associated with radiation and scattering of EM waves.

These results are also the preamble to the analysis of the possibilities of extending this *complex methodology* to the resolution of some scattering problems, in which the appearance of complex scattering laws is guaranteed. Their complete understanding will necessarily require of a deep step by step analysis procedure of all the quantities involved; in fact, this paper is intended to summarize the results corresponding to a first example of that step by step procedure. For instance, the presented results may be validated when

the scattering structure is a finite strip along y-direction, which extends from $-W/2$ to $W/2$ along x-direction, if the strip width is large enough versus the wave length $W/\lambda \gg 1$ in such a way that the physical optics approximation may be used for the induced currents. The studies concerning this problem up to now, reveal that complex versions of both the reflection and diffraction laws appear naturally. The results presented in this paper become essential when trying to generalize the complex parameterization methodology to the analysis of the scattered fields due to complex located induced sources in more complex structures.

ACKNOWLEDGMENT

This work has been supported by the Spanish CICYT under grant TEC2006-12254-C02 (30 % internal funding, 70 % FEDER funding).

APPENDIX A. COMPLEX PARAMETERIZATIONS

A.1. Real Space Parameterization

The real space, Fig. 3, must be parameterized into the SCDS, the SCD, and the $\cos\boldsymbol{\theta}$-plane. This is performed by studying the complex transformations of the beam-referenced axis ξ and η, Fig. 1, when $\xi \gtrless 0$, and $\eta \gtrless 0$. These basic parameterizations provide a clear description of the regions of interest where all the problem should be defined in those complex planes. The results may be summarized as follows:

- SCDS, Fig. 4(a): (i) Axis ξ becomes a parabola described by $q' = q''^2/4b^2 - b^2$. Branches $q'' \lessgtr 0$ correspond to $\xi \gtrless 0$, respectively; (ii) Axis η becomes the axis $q'' = 0$ with $q' \geq -b^2$. The values of $q' \in [-b^2, 0]$ correspond to $|\eta| \leq b$, and $q' \geq 0$ corresponds to $|\eta| \geq b$. The real-source location (x_s, z_s), $(\xi, \eta) = (0, 0)$, point S, becomes the point $(-b^2, 0)$.
- SCD, Fig. 4(b): (i) Axis ξ becomes the straight lines $v = \mp b$, corresponding to $\xi \gtrless 0$; (ii) Axis η becomes the segment $u = 0$, $|v| \leq b$ when $|\eta| \leq b$, and the semi-axis $v = 0$, $u \geq 0$ when $|\eta| \geq b$. The real-source location (x_s, z_s), $(\xi, \eta) = (0, 0)$, point S, becomes the points $(0, \mp b)$ for $\xi \gtrless 0$.
- $\cos\boldsymbol{\theta}$-plane, Figs. 6, 7 and 8: (i) Axis ξ becomes the real point $(\gamma', \gamma'') = (-\cos\alpha_i, 0)$; (ii) Axis η becomes the branches of the hyperbolas $(\gamma'/\cos\alpha_i)^2 - (\gamma''/\sin\alpha_i)^2 = 1$ when $|\eta| < b$, and the branches of the hyperbolas $(\gamma'/\sin\alpha_i)^2 - (\gamma''/\cos\alpha_i)^2 = 1$ when

$|\eta| > b$. For $\alpha_i = 0° : \cos\boldsymbol{\theta} = -\cos\boldsymbol{\theta_s}$, the ξ axis becomes the real point $(\gamma', \gamma'') = (1, 0)$, η axis with $|\eta| < b$ becomes the imaginary axis $\gamma' = 0$, $\gamma'' > 0$, and η axis with $|\eta| > b$ becomes the semi-axis $\gamma' > 1$, $\gamma'' = 0$, and $\gamma' < -1$, $\gamma'' = 0$.

A.2. Boundaries of the Approximations.

The different approximations described in Section 3 and Fig. 2 may be parameterized into the complex spaces, and translated into the real space as follows (the analyses on the $\cos\boldsymbol{\theta}$-plane have been omitted in this section for simplicity):

- The limits established by the *complex HF-FF condition* in (11) may be approximated in the SCD by circumferences, Fig. 4(b), centred at the origin, and with the k_0-dependent radius $M_{\mathrm{CFF}} = k_0\sqrt{u^2 + v^2}$ [8]. These circumferences become also circumferences in the SCDS, Fig. 4(a), centred at the origin and with radius $M^2_{\mathrm{CFF}} = k_0^2\sqrt{q'^2 + q''^2}$. In the real space, they become biquadratic curves, Fig. 3, given by,

$$(\xi^2 + \eta^2)^2 + 2b^2(\xi^2 - \eta^2) = \frac{M^4_{\mathrm{CFF}} - k_0^4 b^4}{k_0^4}. \tag{A1}$$

- The limits established by the *paraxial condition* in (13) are defined in the real space by the well known hyperbolas, Fig. 3,

$$\frac{\xi^2 + b^2}{\eta^2} = M_{\mathrm{par}}, \tag{A2}$$

which become parabolas in the SCDS, Fig. 4(a),

$$q' = \frac{1}{4b^4}\frac{M_{\mathrm{par}} + 1}{M_{\mathrm{par}}}q''^2 - b^2\frac{M_{\mathrm{par}} - 1}{M_{\mathrm{par}}}. \tag{A3}$$

In the SCD, Fig. 4(b), the paraxial limits are described by the following parametric expressions,

$$\begin{cases} u = \dfrac{1}{\sqrt{2}}\sqrt{\sqrt{A^2 + 4b^2\xi^2} + A}, \\ v = \dfrac{\mp 1}{\sqrt{2}}\sqrt{\sqrt{A^2 + 4b^2\xi^2} - A}, \\ A = \dfrac{\xi^2(1 + M_{\mathrm{par}}) + b^2(1 - M_{\mathrm{par}})}{M_{\mathrm{par}}}. \end{cases} \tag{A4}$$

In both the SCDS and the SCD, it may be noticed that there are no important differences between the paraxial limits parameterizations and the ξ-axis representation when $M_{\text{par}} \gg 1$. The analysis of the GB solution approximately reduces then to the analysis over the straight lines $v = \mp b$ in the SCD ($M_{\text{par}} = 4$ in the example shown in Fig. 4(b)).

- The limits established by the *HF-FF condition* in (16) applied to a FFCB define the boundaries of constant relative error in the SCD,

$$v = -u \tan\left(\frac{2k_0 u}{nM_{\text{EP}}}\right), \tag{A5}$$

being $n = 1$ and 3 for TE and TM polarizations.

- Finally, the limits established by the *HF-FF condition* in (18) applied to a GB may be further simplified when $\xi_0/b \gg 1$ by neglecting the $\varphi^{\text{e,m}}$ contribution, leading to,

$$M_{\text{SP}} = \frac{\varphi_l}{\varphi_c} = 2\frac{\xi^2 + b^2}{\eta^2} \gg 1. \tag{A6}$$

This condition defines a set of constant relative error hyperbolas in the real space which are related to the PC itself, as long as $M_{\text{SP}} \sim 2M_{\text{par}}$.

Last two conditions have not been depicted to unload the figures.

A.3. Real Observation Points Parameterization

The $z = 0$ plane contains the real points where the induced currents should be studied. It is parameterized in terms of the real distance from the origin to the real source position, $\xi_{i0} = \xi_0(x = 0)$ and the incidence angle α_i, Figs. 1 and 3.

$$\xi = \xi_{i0} - \eta \tan\alpha_i. \tag{A7}$$

For convenience, it will be represented by,

$$\begin{aligned} \xi &= \xi_{i0} + p\sin\alpha_i, \\ \eta &= -p\cos\alpha_i, \end{aligned} \tag{A8}$$

with $p \in (-\infty, +\infty)$ related to $\xi \in (-\infty, +\infty)$. The translation of the complex source into the SCD (points S in Fig. 4(b)) into the real

space as virtual sources located at $\eta = \pm b$, Fig. 3, leads to the angular restriction,

$$\alpha_i \in [0, \alpha_{i,\max}], \quad \alpha_{i,\max} = \tan^{-1}\left(\frac{\xi_{i0}}{b}\right), \tag{A9}$$

being $\alpha_{i,\max}$ the maximum value of α_i when $\eta = +b$ reaches the $z = 0$ plane, Fig. 3(d). The analysis for $\alpha_i < 0$ is completely similar due to the symmetry of the problem with respect to the z-axis. Examples with $\xi_{i0n} = \xi_{i0}/b = 1.5$, and $\alpha_i = 0^{\rm o}$, 30°, 48.19° and $\alpha_{i,\max} = 56.31^{\rm o}$ are depicted in Figs. 3 and 4, and three of these in Figs. 6, 7 and 8.

- SCDS: by using the relations in (22), the expression in (A7) may be translated into the SCDS, leading to parabolas described by,

$$q' = a_1 q''^2 + a_2 q'' + a_3 \rightarrow \begin{cases} a_1 = \dfrac{1}{4b^2 \sin^2\alpha_i}, \\ a_2 = \dfrac{\xi_{i0}}{b\tan^2\alpha_i}, \\ a_3 = \dfrac{\xi_{i0}^2}{\tan^2\alpha_i} - b^2. \end{cases} \tag{A10}$$

These parabolas may be also described by their vertices (labelled as A in Fig. 4(a)) located at,

$$(z_{1\rm A}, z_{2\rm A}) = (\xi_{i0}^2\cos^2\alpha_i - b^2, -2b\xi_{i0}\cos^2\alpha_i), \tag{A11}$$

their q'-crosses (labelled as B in Fig. 4(a)),

$$(z_{1\rm B}, z_{2\rm B}) = (a_3, 0) = \left(\tfrac{\xi_{i0}^2}{\tan^2\alpha_i} - b^2, 0\right), \tag{A12}$$

and their q''-crosses (labelled as C, $\rm C_1$ and $\rm C_2$ in Fig. 4(a)) that may be summarized as follows: (i) no crosses if $b^2 < \xi_{i0}^2\cos^2\alpha_i$, (examples with $\alpha_i = 0^\circ$ and $\alpha_i = 30^\circ$); (ii) one cross (point C) equal to,

$$(z_{1\rm C}, z_{2\rm C}) = (0, -2b\xi_{i0}\cos^2\alpha_i) = \left(0, \tfrac{-2b^3}{\xi_{i0}}\right), \tag{A13}$$

which corresponds to the vertex of the parabola, point A in (A11), when $b^2 = \xi_{i0}^2\cos^2\alpha_i$ (example with $\alpha_i = 48.19^\circ$), and (iii) two crosses when $b^2 > \xi_{i0}^2\cos^2\alpha_i$ (example with $\alpha_i = \alpha_{i,\max} = 56.31^\circ$). In this case, the limit will occur when $\alpha_i = \alpha_{i,\max}$ in (A9), points $\rm C_1$-$\rm C_2$ in Fig. 4(a), leading to,

$$\begin{aligned} &(z_{1\rm C_1}, z_{2\rm C_1}) = (0, 0), \\ &(z_{1\rm C_2}, z_{2\rm C_2}) = (0, -4b\xi_{i0}\cos^2\alpha_{i,\max}). \end{aligned} \tag{A14}$$

The vertex A in (A11) reduces now to,

$$(z_{1\mathrm{A}}, z_{2\mathrm{A}}) = (-b^2\cos^2\alpha_i, -2b\xi_{i0}\cos^2\alpha_i). \tag{A15}$$

Notice also that (A10) becomes the straight line $q'' = -2b\xi_{i0}$ for normal incidence ($\alpha_i = 0$); the vertex A in (A11) reduces now to $z_{1\mathrm{A}} = \xi_{i0}^2 - b^2$ corresponding to the intersection of $q'' = -2b\xi_{i0}$ and the limiting parabola associated with the ξ-axis in the SCDS.

- SCD: by using the relations in (21) together with (A10), the following parametric expressions are obtained,

$$\begin{cases} u = \dfrac{1}{\sqrt{2}}\sqrt{\sqrt{B^2 + 4b^2B'} + B}, \\ v = \dfrac{\mp 1}{\sqrt{2}}\sqrt{\sqrt{B^2 + 4b^2B'} - B}, \\ B = \xi_{i0}^2 - b^2 + p^2 + 2p\xi_{i0}\sin\alpha_i, \\ B' = \xi_{i0}^2 + p^2\sin^2\alpha_i + 2p\xi_{i0}\sin\alpha_i. \end{cases} \tag{A16}$$

The translation of points A in (A11), and B in (A12), Fig. 4(a), into the SCD, Fig. 4(b), are given by,

$$\begin{cases} u_{\mathrm{A}} = \dfrac{1}{\sqrt{2}}\sqrt{\sqrt{C^4 + b^4 + 2b^2C^2D} + E}, \\ v_{\mathrm{A}} = \dfrac{\mp 1}{\sqrt{2}}\sqrt{\sqrt{C^4 + b^4 + 2b^2C^2D} - E}, \\ C = \xi_{i0}\cos\alpha_i,\ D = 2\cos^2\alpha_i - 1, \\ E = C^2 - b^2. \end{cases} \tag{A17}$$

and

$$(u_{\mathrm{B}}, v_{\mathrm{B}}) = (\sqrt{a_1}, 0). \tag{A18}$$

The unique q''-cross in (A13) when $b^2 = \xi_{i0}^2\cos^2\alpha_i$ will be given in the SCD by,

$$(u_{\mathrm{C}}, v_{\mathrm{C}}) = (u_{\mathrm{C}}, -u_{\mathrm{C}}), \quad u_{\mathrm{C}} = \sqrt{b\xi_{i0}}\cos\alpha_i, \tag{A19}$$

and the two q''-crosses in (A14) when $b^2 > \xi_{i0}^2\cos^2\alpha_i$ and $\alpha_i = \alpha_{i,\max}$ will be given in the SCD by,

$$\begin{aligned} &(u_{\mathrm{C}_1}, v_{\mathrm{C}_1}) = (0, 0), \\ &(u_{\mathrm{C}_2}, v_{\mathrm{C}_2}) = (u_{\mathrm{C}_2}, -u_{\mathrm{C}_2}), \\ &u_{\mathrm{C}_2} = \sqrt{b\xi_{i0}}\cos\alpha_{i,\max}. \end{aligned} \tag{A20}$$

The case for normal incidence is obtained by considering $B = \xi_{i0}^2 + \eta^2 - b^2$ and $B' = \xi_{i0}$ in (A16); the points in the real space with the same value of $|\eta|$ become a unique point (u, v), and the vertex A reduces to $(u_{\mathrm{A}}, v_{\mathrm{A}}) = (\xi_{i0}, -b)$.

- $\cos\boldsymbol{\theta}$-plane: by using (24), the parametric expression of the real observation points will be given by,

$$\begin{aligned} \gamma' &= \frac{-\xi_{i0}u + bv}{u^2 + v^2}\cos\alpha_i, \\ \gamma'' &= \frac{\xi_{i0}v + bu}{u^2 + v^2}\cos\alpha_i. \end{aligned} \tag{A21}$$

This curve always crosses the point $(\gamma', \gamma'') = (-\cos\alpha_i, 0)$ which corresponds to the real point $(\xi_{i0}, 0)$ in the ξ-axis. When $\alpha_i > 0$, the conductor plane always intersects with the positive η-axis in $\eta_c > b$, which becomes the intersection in the $\cos\boldsymbol{\theta}$-plane with the hyperbolic branch in,

$$\begin{aligned} \gamma' &= \frac{-\xi_{i0}\cos\alpha_i}{\sqrt{\eta_c^2 - b^2}}, \\ \gamma'' &= \frac{b\cos\alpha_i}{\sqrt{\eta_c^2 - b^2}}. \end{aligned} \tag{A22}$$

If $\alpha_i = \alpha_{i,\max}$, the point $\eta = b$ touches the $z = 0$ plane, point which goes to infinity in the $\cos\boldsymbol{\theta}$-plane. Finally, for any value of α_i, when $\eta \to \pm\infty$, that is $x \to \pm\infty$, these points are seen with angles $\boldsymbol{\theta} \to \pi/2$ and $3\pi/2$, respectively, leading to points for which $\cos\boldsymbol{\theta} = 0$ are real. Figs. 6, 7 and 8 show examples for the cases with $\alpha_i = 48.19°$, $0°$, and $\alpha_{i,\max} = 56.31°$.

APPENDIX B. LIST OF ACRONYMS

CB:	Complex Beam.
EP-FFCB:	Elliptical Phase Far Field Complex Beam.
FF-CB:	Far Field Complex Beam.
GB:	Gaussian Beam.
HF-FF:	High Frequency-Far Field.
PC:	Paraxial Condition.
SCD:	Space of Complex Distances.
SCA:	Space of Complex Angles.
SCDS:	Space of Complex Distances Squared.
SP-GB:	Straight Phase Gaussian Beam.

REFERENCES

1. Deschamps, G. A., "Gaussian beam as a bundle of complex rays," *Electron. Lett.,* Vol. 7, 684–685, 1971.
2. Felsen, L. B., "Complex rays," *Philips Res. Repts.* Vol. 30, 187–195, 1975.
3. Ra, J. W., H. L. Bertoni, and L. B. Felsen, "Reflection and transmission of beams at a dielectric interface," *SIAM J. Appl. Math.,* Vol. 24, No. 3, 396–413, 1973.
4. Lu, I. T., L. B. Felsen, and Y. Z. Ruan, "Spectral aspects of the Gaussian beam method: reflection from a homogeneous half-space," *Geophys. J. R. Astr. Soc.,* 915–932, 1987.
5. Dahl, M., "Electromagnetic Gaussian beams and Riemannian geometry," *Progress In Electromagnetics Research*, PIER 60, 265–291, 2006.
6. Kaiser, G., "Physical wavelets and their sources: real physics in complex spacetime," *J. Phys. A: Math. Gen.*, Vol. 36, 291–338, 2003.
7. González-Morales, M. J., C. Dehesa-Martínez, and E. Gago-Ribas, "About complex extensions and their application in electromagnetics," *Complex Computing-Networks. A link between Brain-like and Wave-oriented Electrodynamic Algorithms,* I. C. Gknar and L. Sevgi (eds.), Springer Proceedings in Physics, Vol. 104, 81–86. Springer-Verlag, 2006.
8. Gago-Ribas, E., M. J. González-Morales, C. Dehesa-Martínez, "Analytical parametrization of a 2D real propagation space in terms of complex electromagnetic beams," *IEICE Trans. on Electronics*, Special Issue on Electromagnetic Theory—Scattering and Diffraction, Vol. E80-C, No. 11, 1434–1439, Japan, November 1997.
9. Gago-Ribas, E. and M. J. González-Morales, "2D complex point source radiation problem. I. Complex distances and complex angles," *Turkish Journal of Electric Engineering and Computer Sciences*, Special Issue on Electromagnetic Problems and Numerical Simulation Techniques: Current Status - Future Trends,Vol. 10, No. 2, 317–343, 2002.
10. González-Morales, M. J. and E. Gago-Ribas, "2D complex point source radiation problem. II. Complex beams," *Turkish Journal of Electric Engineering and Computer Sciences*, Special Issue on Electromagnetic Problems and Numerical Simulation Techniques: Current Status - Future Trends, Vol. 10, No. 2, 345–369, 2002.

11. Heyman, E. and L. B. Felsen, "Gaussian beam and pulsed-beam dynamics: complex-source and complex-spectrum formulations within and beyond paraxial asymptotics," *J. Opt. Soc. Am. A,* Vol. 18, No. 7, 1588–1611, 2001.
12. Martini, E., G. Pelosi, and S. Selleri, "Line integral representation of physical optics scattering from a perfectly conducting plate illuminated by a Gaussian beam modeled as a complex point source," *IEEE Trans. on AP,* Vol. 51, No. 10, 2003.
13. Lin, W. and Z. Yu "Existence and uniqueness of the solutions in the SN, DN and CN waveguide Theories," *J. of Electromagn. Waves and Appl.*, Vol. 20, No. 2, 237–247, 2006.
14. Imram, A. and Q. A. Naqvi, "Diffraction of electromagnetic plane wave by an impedance strip," *Progress In Electromagnetics Research*, PIER 75, 303–318, 2007.
15. Abo-Seida O. M., "Far-field due to a vertical magnetic dipole in sea," *J. of Electromagn. Waves and Appl.*, Vol. 20, No. 6, 707–715, 2006.
16. Arnold M. D., "An efficient solution for scattering by a perfectly conducting strip grating," *J. of Electromagn. Waves and Appl.*, Vol. 20, No. 7, 891–900, 2006.
17. Watanabe, K. and K. Yasumoto, "Two-dimensional electromagnetic scattering of non-plane incident waves by periodic structures," *Progress In Electromagnetics Research*, PIER 74, 241–271, 2007.
18. Hussain, W., "Asymptotic analysis of a line source diffraction by a perfectly conductiong half plane in a bi-isotropic medium," *Progress In Electromagnetics Research*, PIER 58, 271–283, 2006.
19. Gago-Ribas, E., M. J. González-Morales, and C. Dehesa-Martínez, "Challenges and perspectives of complex spaces and complex signal theory analysis in electromagnetics: First steps," *Electromagnetics in a Complex World: Challenges and Perspectives,* I. M. Pinto, V. Galdi, and L. B. Felsen (eds.) Springer Proceedings in Physics, Vol. 96, 175–188. Springer-Verlag, 2003.
20. Abramowitz, M. and I. A. Stegun, *Handbook of Mathematical Functions,* Eq. (9.2.3), Dover Pub., New York, 1965.